Chapter 17

Experimental Study of Standard Aeration Efficiency in a Bubble Column

Florentina Bunea and Gabriel Dan Ciocan

Additional information is available at the end of the chapter

http://dx.doi.org/10.5772/intechopen.76696

Abstract

Water aeration is a major feature in many industrial applications, for example, hydraulic turbines, fish farms, water treatment, and so on. A key consideration is the efficiency of the aeration itself, that is, the effectiveness of the transfer of oxygen from air to water in relation to the energy consumed by injection. In this chapter, several configurations of the aerator are analyzed for overall efficiency optimization. Two different parameters are investigated (the arrangement of aeration apertures and aperture diameters between 0.2 and 1.6 mm) using aerators with perforated metal plates and, for comparison, ceramic and fritted (sintered) glass plates. For the arrangement of the apertures on the perforated metal plates, bubble coalescence and contraction coefficients are measured. Each configuration's results (Kla, SOTR, SAE) are compared and analyzed.

Keywords: standard aeration efficiency, oxygen transfer, bubble column, aerator, standard oxygen transfer rate, aeration optimization

1. Introduction

Oxygen transfer in water is a key component in environmental technologies, for example, in wastewater treatment, by virtue of the efficiency of the transfer of oxygen and the total costs of the air injection process, and water treatment itself is common in many industrial applications, for example, in the chemical, hydraulic, and nuclear industries, for which biphasic air-water flow characterization is required for each particular case. For example, for water treatment, energy consumption is the highest for aeration processes, as compressed air is an expensive working medium. The same behavior occurs in aeration for biological purposes, for example in fish farming, or in water aeration downstream of

hydraulic turbines, in which the design of the aeration systems (orifice diameter, configuration, operating conditions, and location) may significantly improve the quality of turbine aeration [1, 2]. The aerator design parameters are used to determine the best balance between oxygen transfer (volume of air injected and size and shape of generated bubbles) and energy consumption.

Aerators (spargers) can be made from porous ceramic or metallic materials, fritted (sintered) glass, or plastic, each having specific features in emitting bubbles to increase the contact surface between the gas and the liquid.

In literature, the volumetric mass transfer coefficient Kla was also obtained in situ, [3–6], for different configurations. As the configuration and operating conditions are far from this experiment, a direct comparison cannot be performed.

The main objective of this study is to optimize an aeration device, that is, to achieve the best dissolved oxygen (DO) transfer versus minimized energy consumption for injection. The classical experiment of an ascending bubble column was used to compare many injection devices. The aeration devices are mainly perforated metallic plates (MPs). Two parameters are studied: orifice size and arrangement. As a control, the active admission area is kept constant for all configurations. The injection air flow rate is controlled and the main aeration parameters (Kla and standard oxygen transfer rates [SOTR]) measured. Comparison of standard aeration efficiency (SAE) is also recorded. The efficiency results are compared with two other aerators, that is, a ceramic plate (CP) and a glass plate (GP). Finally, the optimized configuration in terms of SAE (best compromise between dissolved oxygen transfer and energy consumption for the air injection) is chosen.

2. Experimental setup to study the oxygen transfer of aerators

The setup [7] consists of a rectangular tank (**Figure 1**) with L = 0.3 m, h = 0.88 m, and hydrostatic load H = 0.8 m, filled with 79.2 l of water. In the tank (1) the aerator (2) equipped with interchangeable metallic plates (MPs) is immersed and tested. Upstream of it a flow-meter (3) is connected for measuring the air flow rate through the aerator and a differential manometer (5) for measuring the pressure drop across the aerator. The experimental setup is sized so that the walls of the tank do not affect the mass transfer of the air bubble column to the water ($L = 6 \cdot D$). With the peristaltic pump (6) the water is sampled in the middle of the tank, 2 cm from the wall, avoiding the air bubbles in the DO measuring cell. The water passes through the oximeter (7) and is then reintroduced into the system.

Five interchangeable perforated metallic plates with holes of d = 0.2, 0.3, 0.5, 0.9, 1.6, and 2.4 mm (**Figures 2** and **3**) are tested. To avoid bubble coalescence, the holes are located 10 d apart, and to negate any influence of the contraction coefficient of the hole, its length is 5 d. To increase the active emission area, and implicitly the interface area, the measurements are repeated for a second series of MPs with orifices placed 7 d apart. For both series of tests, the diameter of the MP is D = 44.8 mm. The aerator intake has a conical shape to ensure uniform air repartition at the intakes of the aeration holes.

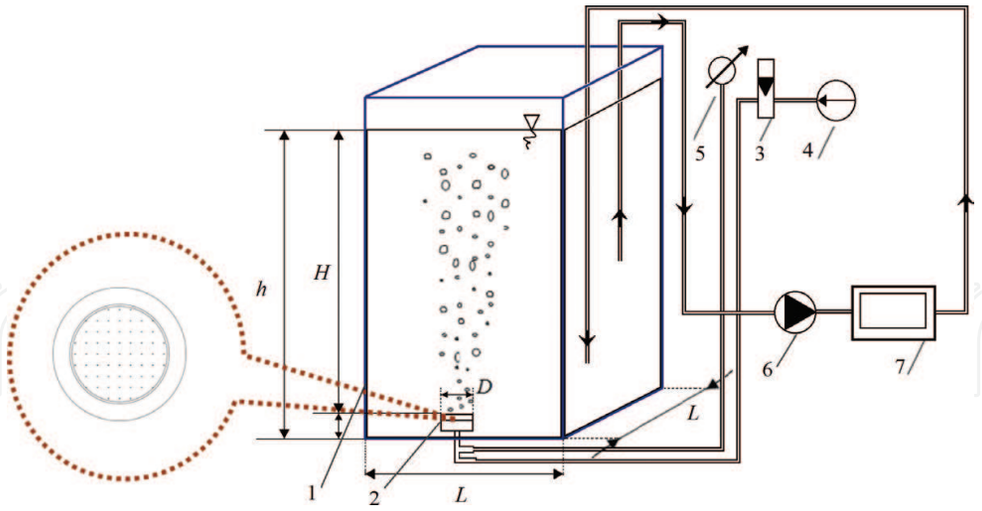

Figure 1. Experimental setup (1–tank, 2–aerator, 3–flow-meter, 4–air compressor, 5–manometer, 6–peristaltic pump, 7–oximeter, MP–interchangeable metallic plate).

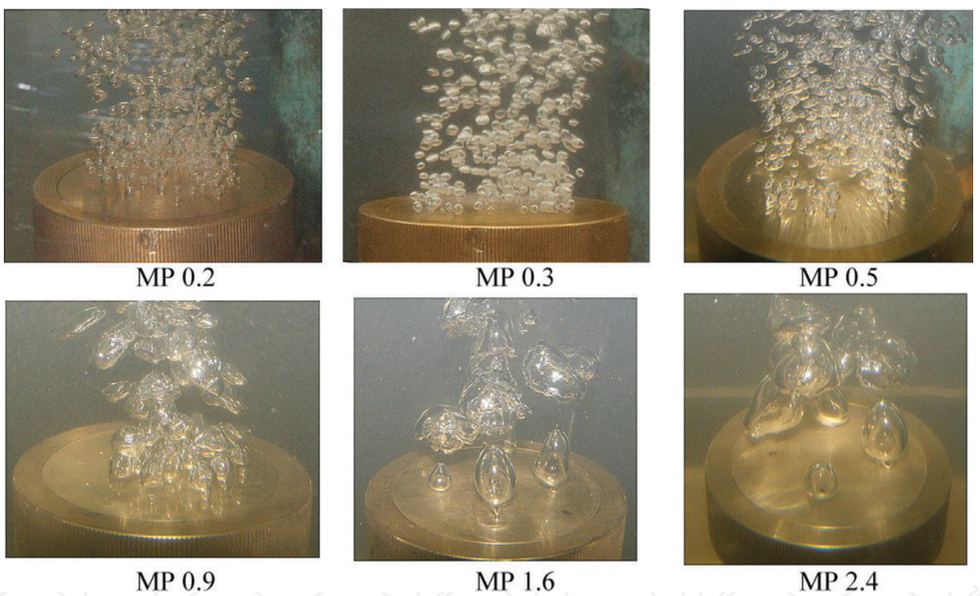

Figure 2. Tested metallic plates in operation.

In **Table 1** the geometric characteristics of MPs, series 1 and 2, are presented. The last column shows, in bold, the theoretical air-water interface area at the outlet of the bubble from the injection aperture. The design of MP in the second series increases the air-water interfacial area (***a***) at the bubbles outlet by up to 2.5 times (**Table 1**).

The initial radius (R_0) of an air bubble at its detachment from the hole of an aerated system immersed at a depth H is calculated from the balance of the Archimedean and superficial tension forces, neglecting the weight of the air in the bubble [8].

$$R_0 = \left(\frac{3}{4} \cdot \frac{d\sigma}{\rho g}\right)^{1/3} \tag{1}$$

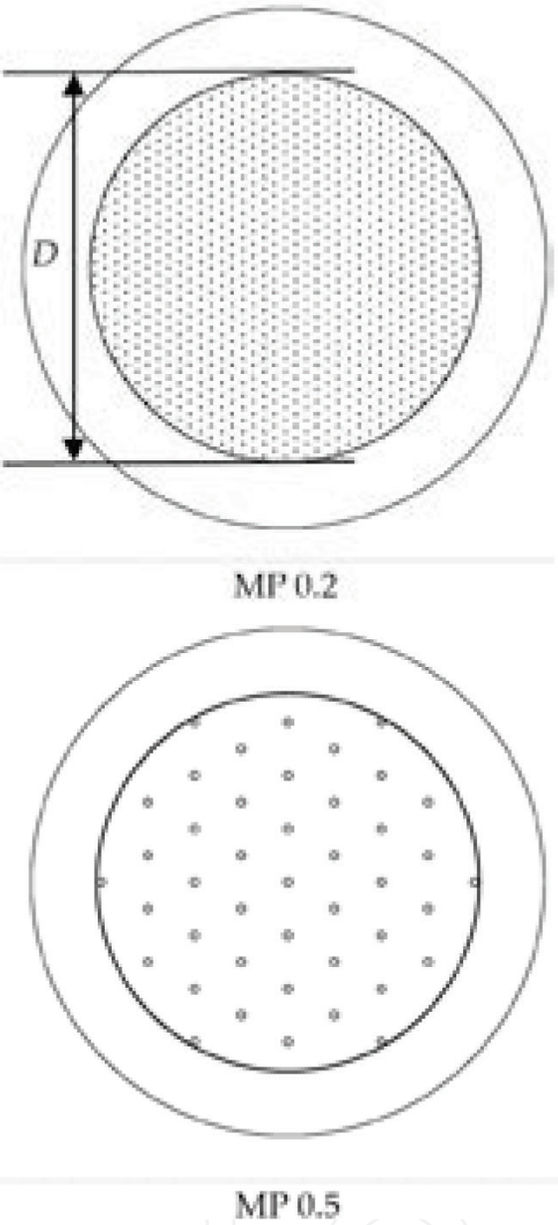

Figure 3. Layout of holes for 7*d* arrangement for 0.1 and 0.5 mm hole diameter.

The interface area (a) of the first swarm of bubbles is considered spherical at the time of detachment and is calculated with the relationship shown in Eq. (2). The active area of the intake of the air into water is calculated with the relationship (3).

$$a = n \cdot \pi R_0^2. \tag{2}$$

$$s = n \cdot \pi d^2/4 \tag{3}$$

The interface area (***a***) increases in the second series by up to 2.8 times (**Table 2**).

d (mm)		N		R_0 (mm)		s (mm²)		s' (%)		a (mm²)		$\frac{a_{S2}}{a_{S1}}$
S1	**S2**	**S1**	**S2**	**S1**	**S2**	**S1**	**S2**	**S1**	**S2**	**S1**	**S2**	
2.4	—	4	—	2.38	—	18.1	—	1.1	—	285	—	—
1.6	1.6	6	14	2.08	2.08	12.1	28.1	0.8	1.8	326	761	**2.33**
0.9	0.9	21	43	1.72	1.72	13.4	27.4	0.9	1.7	781	1599	**2.05**
0.5	0.5	61	151	1.41	1.41	12.0	29.6	0.8	1.9	1524	3772	**2.47**
0.3	0.3	177	414	1.19	1.19	12.5	29.3	0.8	1.9	3150	7367	**2.34**
0.2	0.2	385	951	1.04	1.04	12.1	29.9	0.8	1.9	5233	12,926	**2.47**

Table 1. Emission performance of the two series of metallic plates S1 and S2.

MP	V_{void} (l)	n_b (–)	ε (%)
MP 1.6	0.25	2953	0.347
MP 0.9	0.26	4601	0.361
MP 0.5	0.27	8449	0.375
MP 0.3	0.28	15,905	0.389
MP 0.2	0.29	27,403	0.403
MP 0.1	0.3	42,468	0.417

Table 2. Void fraction for the second series of plates at Q = 0.1 l/s.

For the theoretical evaluation of the interfacial area (a_i) of all the bubbles in the system an air flow rate Q = 0.1 l/s is injected in water. By measuring the contact time of air bubbles in water (T) and the sudden shutdown of the air supply, the void volume from the system is obtained: $V_{void} = T \cdot Q$. The interfacial area of the all bubbles in the system is calculated using relationship (4)

$$a_i = n_b \cdot A_b = \frac{3TQ}{R_0}. \tag{4}$$

The average global void fraction is calculated using relationship (5)

$$\varepsilon = \frac{V_{void}}{V} 100. \tag{5}$$

The experimental results of the mass transfer of the two sets of plates are presented in the next chapter.

3. Volumetric mass transfer coefficient corresponding with energy consumption

To obtain the oxygen transfer the following configurations are tested:

- series 1 of five metallic plates (MP 0.2, MP 0.3, MP 0.5, MP 0.9, and MP 1.6);
- series 2 of two metallic plates (MP 0.2 and MP 0.5);
- a ceramic plate (CP) with volume porosity in the range 45–50%; and
- a fritted (sintered) glass plate (GP) with porosity controlled in the range 0.25–0.315 μm.

For all series of metallic plates, the following injected air flow rates are tested: Q = 180, 360, 480, 600, 720, 960, 1140 l/h. The results are then compared with the aeration performance of the CP and GP.

The method of measuring dissolved oxygen (DO) in clean water, according to the standard for measuring oxygen transfer in water [9], requires removing DO from water (using Na_2SO_3) and then reoxygenating up to at least 90% of the saturation concentration value. To obtain standard oxygen transfer rates (SOTR), the water in which testing takes place must be qualitatively equivalent to drinking water. Concentration of dissolved oxygen in time (C) is measured while maintaining constant air flow injected into the system. The measurements are repeated for each of the air flow rates with the abovementioned plates. After each set of measurements, the standard procedure is applied for the removal of DO from water and reoxygenation up to 90% of the saturation concentration value.

3.1. Processing of the experimental data

The following is an example of estimating the Kla and C_s parameters for the plate MP 1.6 operating at an injection air flow rate of Q = 360 l/h. The concentration of DO in time C = f(t) is shown in the figure (**Figure 4**).

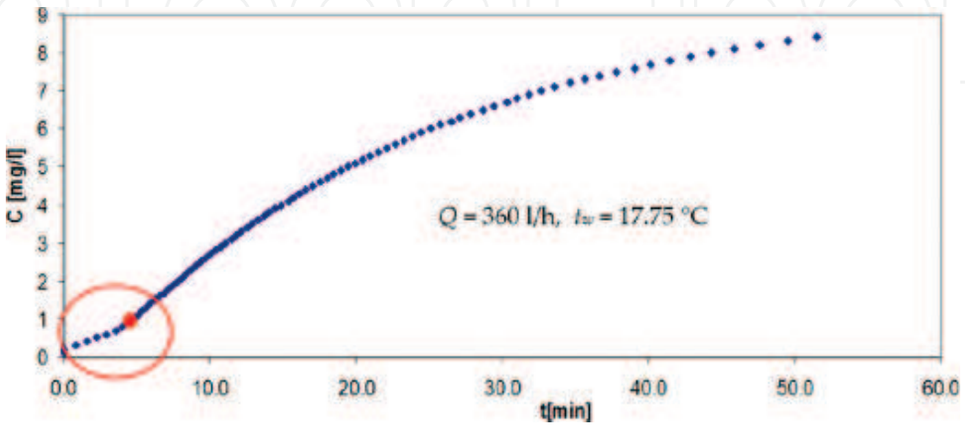

Figure 4. C = f(t) and the inflection point detection.

http://dx.doi.org/10.5772/intechopen.76696

In the event of an inflection point (marked in red in **Figure 4**), it is allowed to truncate the curve up to the concentration at $C = 1.5 \cdot C_i$, where C_i represents the concentration corresponding to the inflection point. If the curve does not have an inflection point, the data can be truncated to 20% of the C_s.

To obtain time delay, the remaining data are extrapolated through the intersection of the fitted curve at the time axis (**Figure 5**). The primary data are corrected by shifting the curve to the initial moment that the concentration of dissolved oxygen is zero—see **Figures 5** and **6**.

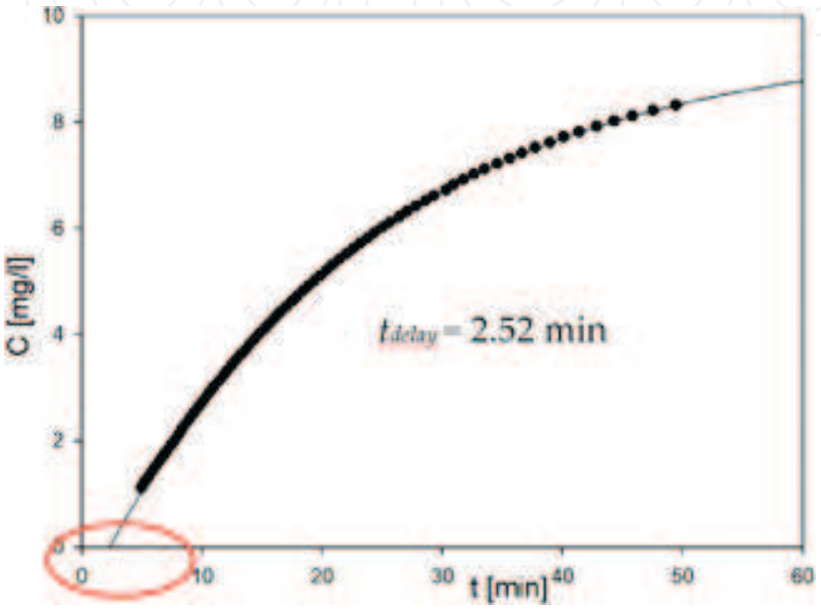

Figure 5. Extrapolation of experimental data to obtain the delay time, for MP 1.6, at Q = 360 l/h.

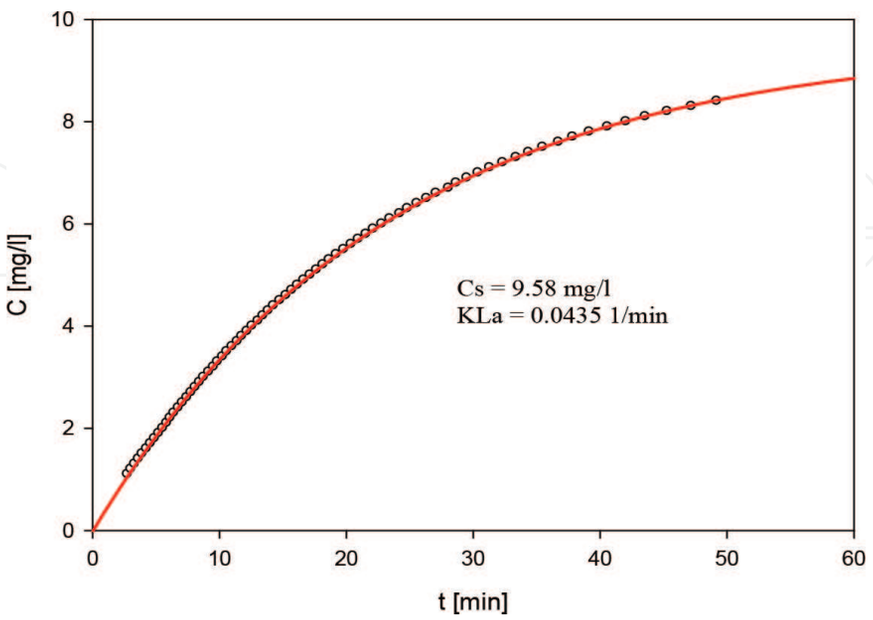

Figure 6. Estimation of Kla and *Cs* parameters by non-linear regression for MP 1.6, at *Q* = 360 l/h.

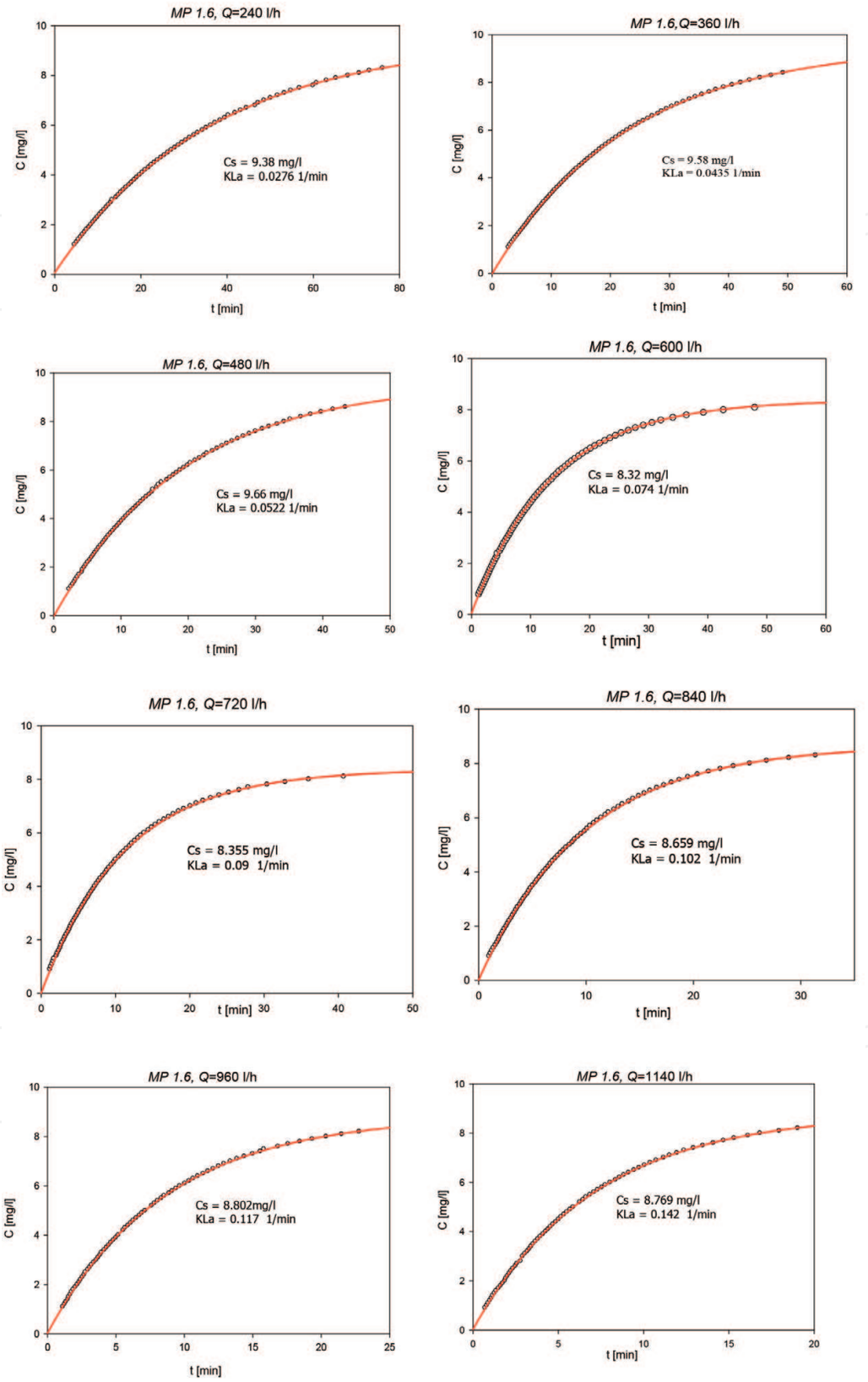

Figure 7. Estimation of Kla and Cs parameters by non-linear regression for MP 1.6.

The chart (**Figure 5**) is replotted with corrected data using the mathematical model described by Eq. (6):

$$C = C_S - (C_S - C_0)\, e^{-klat} \tag{6}$$

The Kla and C_s parameters are obtained (**Figure 6**).

The procedure is repeated for all the test plates for the air flow rate range: Q = 96–1140 l/h.

Figures 7 and **8** show the graphs for Kla and C_s estimation of MP 0.5 and MP 1.6 at injected air flow rates, Q = 240÷1140 l/h.

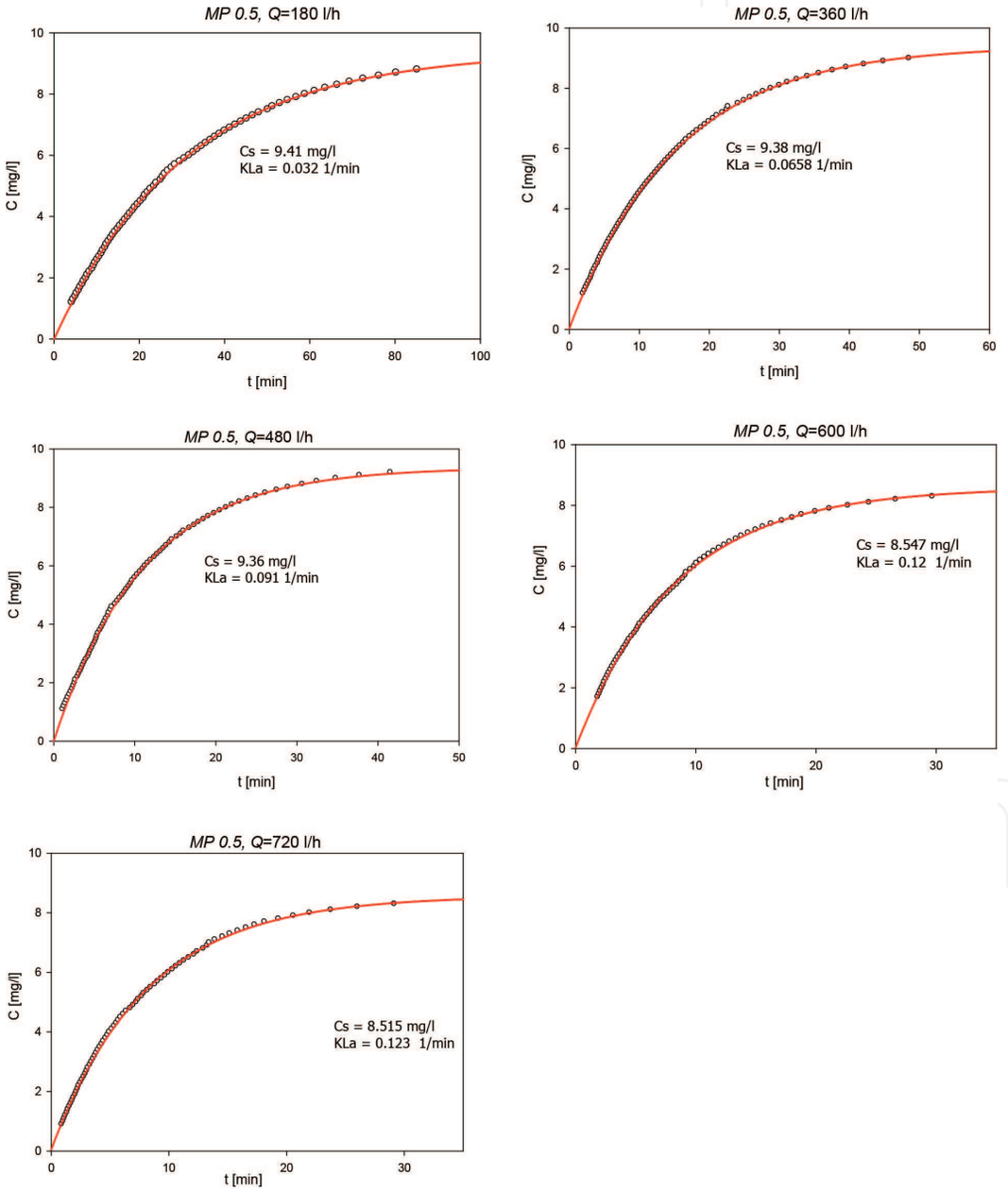

Figure 8. Estimation of Kla and *Cs* parameters by non-linear regression for MP 0.5.

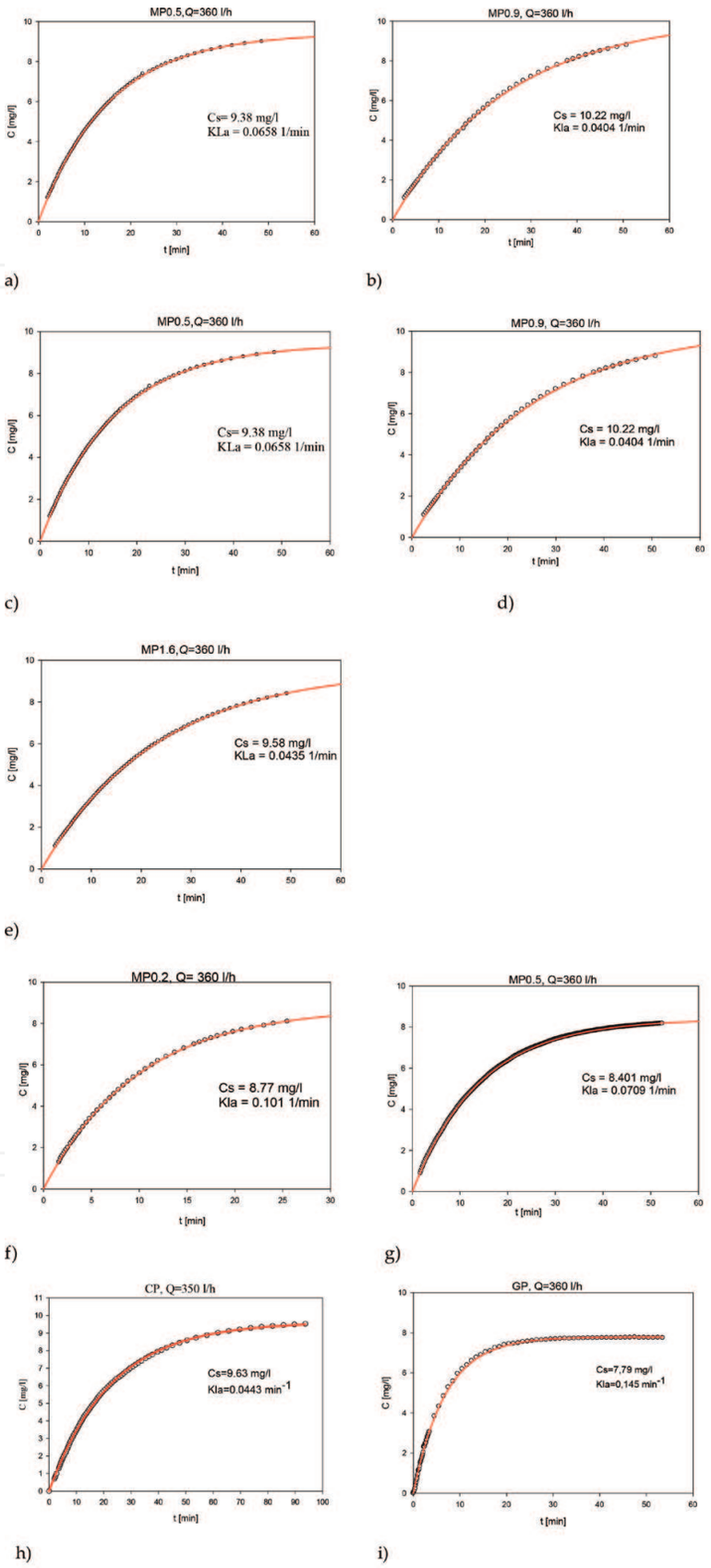

Figure 9. Estimation through nonlinear regression of Kla and Cs parameters for Q = 360 l/h. (a) MP 0.2, series 1. (b) MP 0.3, series 1. (c) MP 0.5, series 1. (d) MP 0.9, series 1. (e) MP 1.6, series 1. (f) MP 0.2, series 2. (g) MP 0.5, series 2. (h) Ceramic plates with volume porosity in the range 45÷50%. (i) Glass plates with porosity controlled in the range 0.25÷0.315 μm.

http://dx.doi.org/10.5772/intechopen.76696

The regression curves for the estimated parameters Kla and *Cs* for all nine tested plates at the injection flow rate Q = 360 l/min are presented for comparison in **Figure 9**.

From the aeration point of view (dissolved oxygen transfer), an improvement is observed between the first and second series of the MP, the second giving a better performance as the interphase area is higher. However, the MP aeration characteristics Kla and *Cs* are lower compared with CP and GP. GP provides the best aeration characteristics.

Krishna and van Baten [10] illustrate the influence of column diameter on Kla (**Figure 10**), assuming that a homogeneous flow regime prevails (with dispersion consisting of 5 mm of small-sized bubbles). In this study, the diameter of the aeration device is equal to the diameter of the tank. A strong reduction of aeration characteristics is observed. The bubble column is confined by the walls and the flow velocity induced in the ascending column produces an increased velocity in the air column that tends to accelerate the bubbles in the central core, reducing gas–liquid contact time.

In our study the water column is higher than the bubble column, L/D = 6.8, in order not to have the water column constrained by confinement. For this reason, Kla is less than in the Krishna experiment, for equivalent bubble diameters (MP 0.5) around 5 mm.

The initial theoretical ascending velocity of the bubbles can be calculated using:

$U = Q/A$, where Q [m^3/s] is the air flow rate through the aerator and A [m^2] is the emission surface of the plate (active area). The hypothesis of the uniform initial ascending velocity is a rough estimation, which is more realistic for MP (because of uniform orifice losses) but less so for GP and CP. Krishna and van Baten [10, 11], obtained from CFD, using the effective area of transfer, with large bubbles corresponding to 20 mm are represented in (**Figure 11**) by filled circles, and the 5 mm sized bubbles, are represented by filled squares. The open circles relate to experimentally determined values and $U_{trans,}$ is the transition velocity.

A decrease in the Kla coefficient is observed with an increasing bubble diameter, as transfer performance is related to the interfacial area (for the same air flow rate). However, it is observed that Kla is comparable for two experiments. The difference is explained by the limitation of the bubble column size and the acceleration of the bubble column in Krishna's experiment.

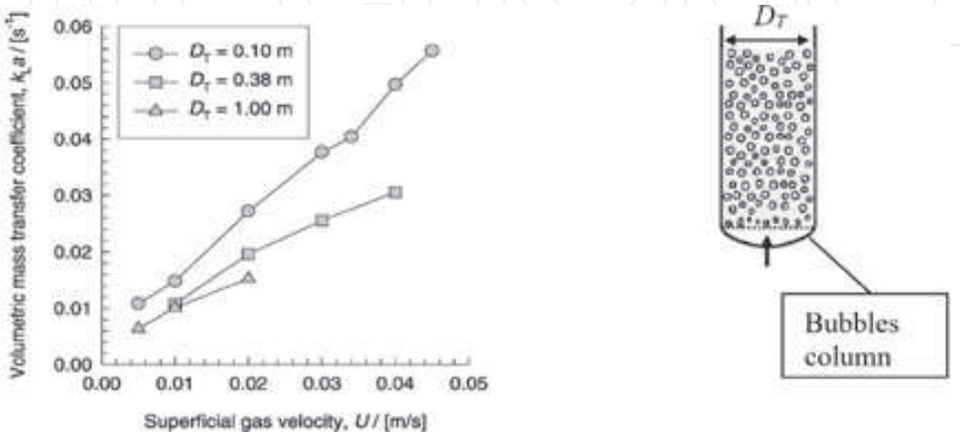

Figure 10. Influence of column diameter DT (by numerical simulations) on Kla coefficient for operation in the homogeneous flow regime [10].

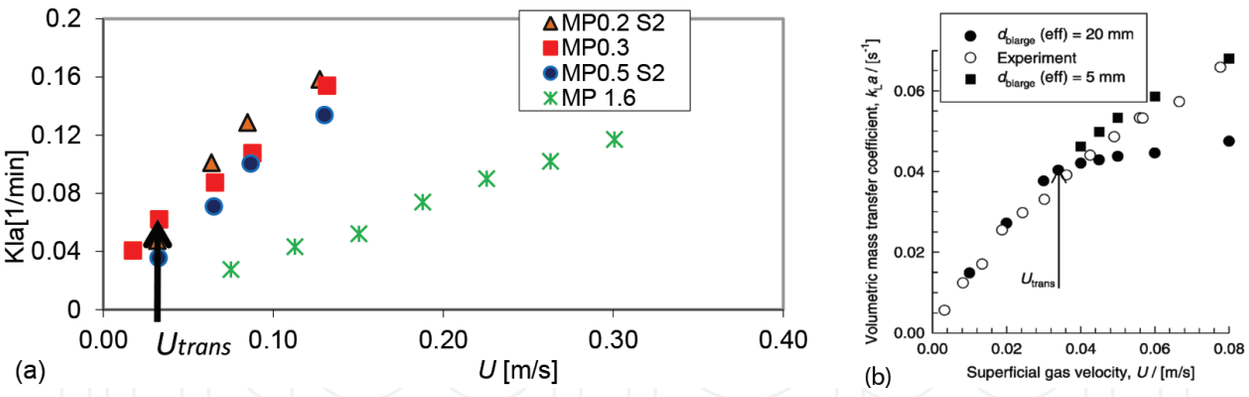

Figure 11. Volumetric mass transfer coefficient as a function of U, from the homogeneous to the heterogeneous flow regime, (a) our experiments, (b) Krishna experiment's [9].

4. Air flow influence on the aeration efficiency

The experimental data were post-processed following standard procedures [9] and reduced to the same temperature and pressure conditions (t_w = 20°C and p_{atm} = 1 atm) in order to ascertain the influence of hole size on the aeration efficiency.

As per the standard process the following steps was considered:

- volumetric mass transfer coefficient, estimated by regression and corrected at 20°C

$$Kla_{20} = Kla \cdot \theta^{|20-t|} \text{ [1/min]} \tag{7}$$

- concentration of DO at the measuring point, at saturation, corrected at temperature 20°C, at standard pressure 101 kPa, and relative humidity conditions are 100%

$$C_{s20} = C_s\left(\frac{1}{\tau\Omega}\right) \tag{8}$$

- standard oxygen transfer rate (*SOTR*)

$$SOTR = kla_{20} \cdot C_{s20} \cdot V \text{ [mg/min]} \tag{9}$$

- standard oxygen transfer efficiency (*SOTE*)

$$SOTE = \frac{SOTR}{W_{O2}} \text{ [–]} \tag{10}$$

- standard aeration efficiency (*SAE*)

$$SAE = \frac{SOTR}{P} \text{ [kg}_{OD}\text{/kWh]} \tag{11}$$

http://dx.doi.org/10.5772/intechopen.76696

The power consumed for the injection of air through the aerator

$$P = Q \cdot (dp + \rho gH)/1000 \quad [\text{kW}] \tag{12}$$

Figure 12 shows the pressure losses measured for all MPs, CPs, and GPs. The injection losses on MPs are 10 times inferior to the CPs and GPs. The losses decrease with increasing diameter of the orifice but in a reduced report compared to CPs and GPs. The arrangement of the holes plays a role, too, with the second series of MPs exhibiting smaller losses at the point of air injection.

Aeration parameters compared with CPs and GPs from the two series of MPs are presented in **Figures 13–18**. The ceramic plate has volume porosity in the range 45–50% and the fritted (sintered) glass plate has a porosity which is controlled in the range 0.25–0.315 μm.

These experiments show that increases in the air flow rate lead to increased dissolved oxygen transfer and Kla up to a certain value, after which Kla remains constant. Increasing the air flow rate induces the losses of air admission increases. In such as way the maximum aeration and minimum energy consumption is optimized, reflected by SAE (**Figure 18**).

Following this analysis, the MP gives the best results compared to the equivalent configurations in CP or GP. The pressure losses are 10 times less important compared with the CP and GP. Reducing the distance between the holes from 10 to 7 diameters, increasing the number of holes for the same active surface, and thus reducing the bubble size lead to an increase in the air-water contact surface and the retention time in water and thereby improves the transfer of dissolved oxygen.

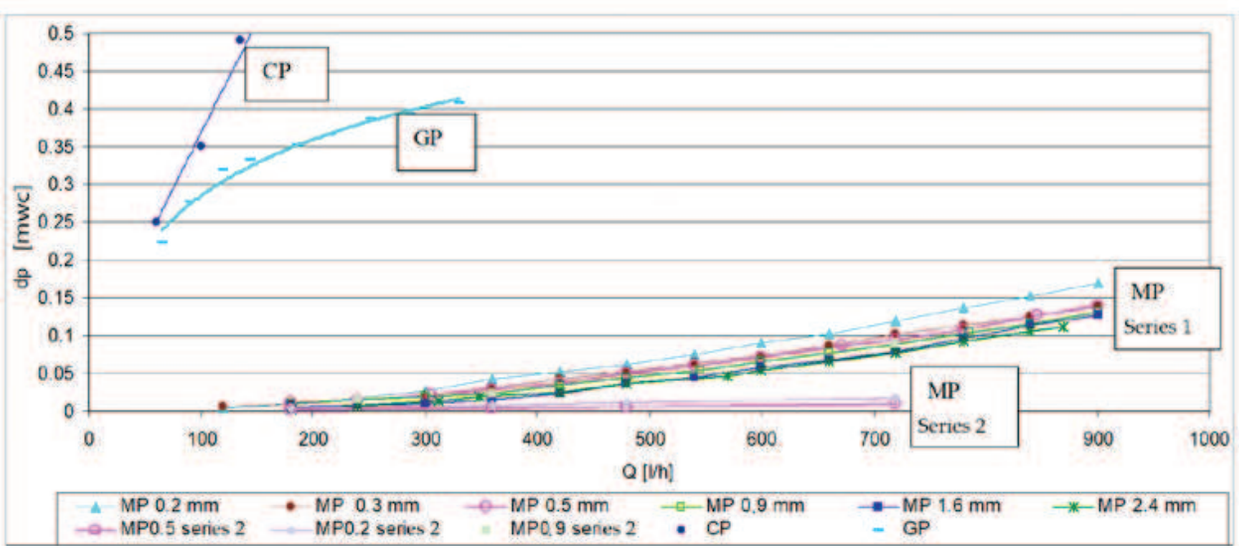

Figure 12. Pressure drop on the aerator variation for different types of plates (MP series 1, MP series 2, ceramic plate CP and glass plate GP).

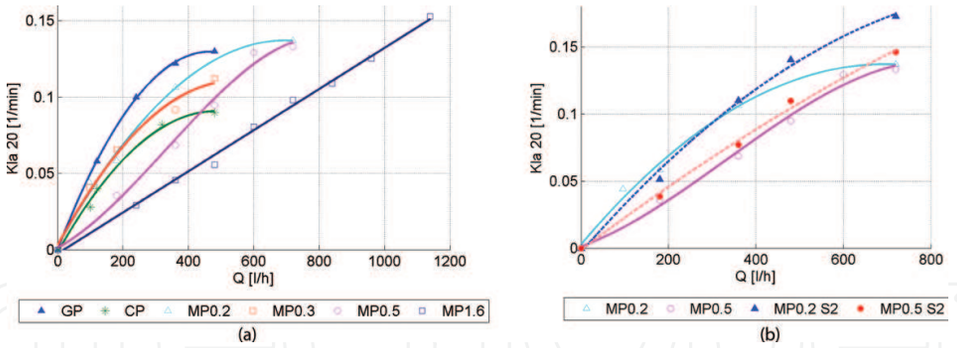

Figure 13. Kla20 variation function of the air flow rate under standard conditions and comparison between the two MP series (right side).

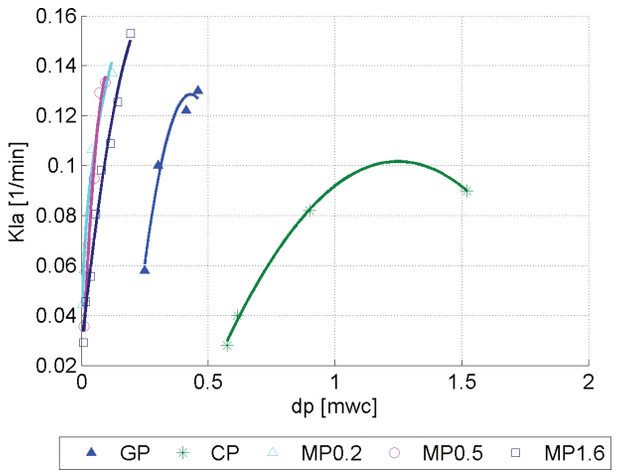

Figure 14. Kla variation function of aerator pressure drop for MP and comparison with GP and CP.

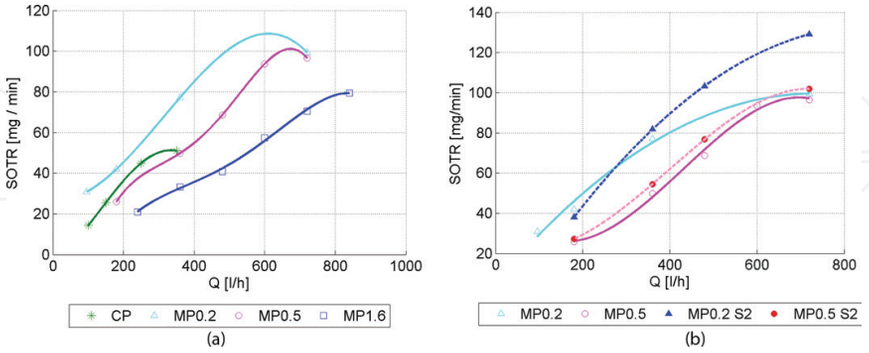

Figure 15. Standard oxygen transfer rate (oxygenation capacity) variation function of injected air flow rate.

Experimental 2D particle image velocimetry (PIV) measurements, with uniform background lighting and laser-induced fluorescence (LIF) of the tracking particles, were performed in order to characterize the air-water biphasic flow and the 2D bubble column rising velocity in static water—see works by Murgan et al. [12]. For complete characterization of the flow, the

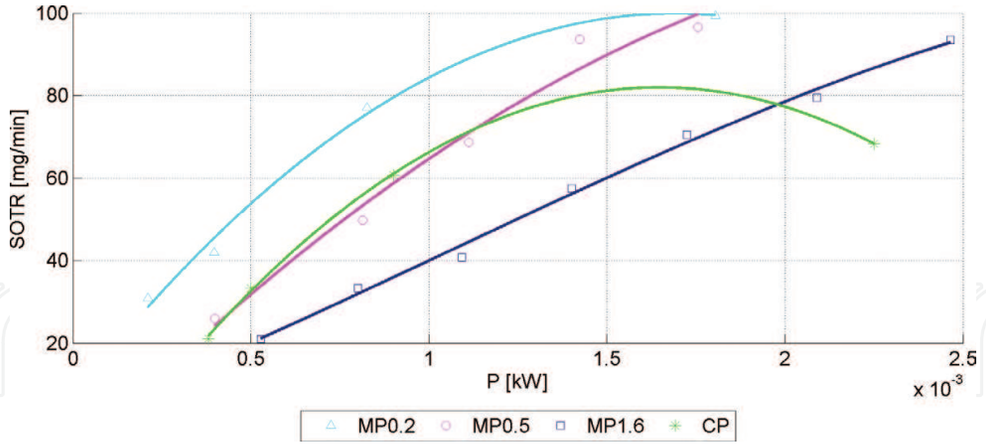

Figure 16. Standard oxygen transfer rate variation function of the power consumed for the air injection through the aerator.

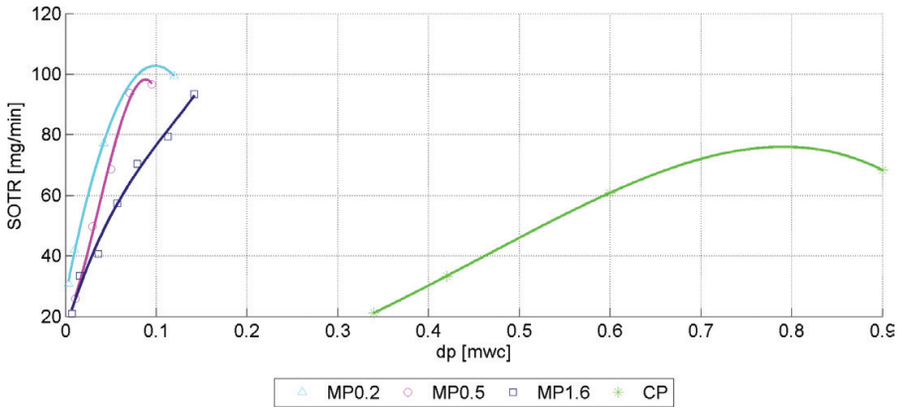

Figure 17. Standard oxygen transfer rate variation function of the aerator pressure drop.

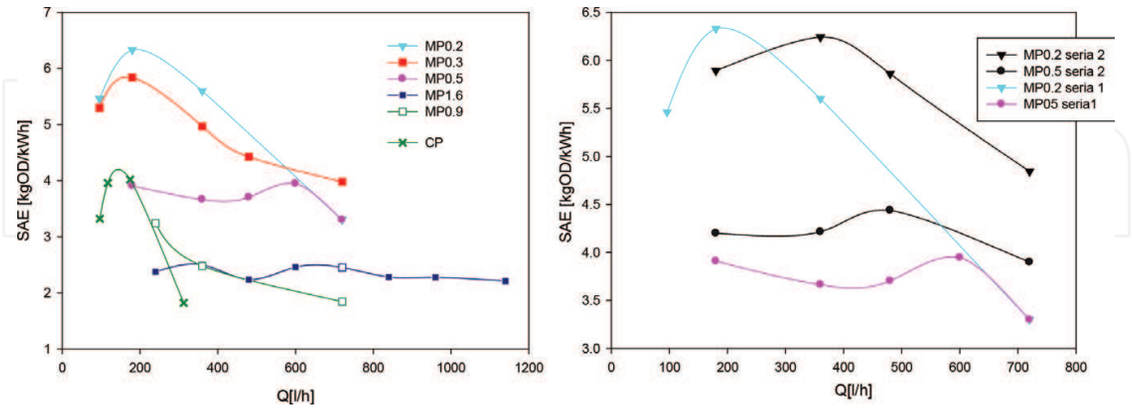

Figure 18. Standard aeration efficiency at different injection air flow rates. Comparison between the two series of MP (right side).

velocity field induced by the column of bubbles and the bubbles features are simultaneously determined using image processing technics. The bubbles features include: ascension velocity, diameter variation, interfacial area and shape factor.

5. Conclusions

This chapter presents an experimental study for the global optimization of aeration in the industrial configuration. For optimization two main parameters were considered: aeration performance (dissolved oxygen transfer) and energy consumption for the air injection.

Was considered many injection devices: two series of metallic plates with different designs (the arrangement of aeration holes, hole shapes, and diameter) and hole diameters between 0.2 and 2.4 mm, ceramic plates, and glass plates in an air bubble column in water. The investigations where performed for the following air flow rates: Q = 180, 360, 480, 600, 720, 960, 1140 l/h. The aeration performances were obtained, using the procedure of the standard procedure ASCE 2-91/1993 (Kla and SOTR), and compared with other literature results. The results are coherent for the tendencies and the differences were explained.

Based on these results and injection loss measurements, the SAE—standard aeration efficiency—was calculated for all plates and global efficiency curves were plotted.

Taking into account these parameters in an aerator design, and optimizing the total efficiency, allows for an efficient deployment of aeration devices in industrial systems. As variations in efficiencies for dissolved oxygen transfer, or losses, in different aeration devices can be greater than a factor of 10, the findings of this optimization study are significant for achieving the best design of aeration systems for hydraulic turbines and in water treatment and so on in regulation to the specific needs and capacity of each application (available air flow rate, pressure of injection, aeration need, etc.).

This study shows the importance of the optimization of the aerator device in terms of materials, aperture arrangement, aperture shape, aperture dimension for the specific conditions of each application (air flow rate, pressure gradient, emplacement of the aeration device), and for the best global efficiency—best compromise between the energy needed for the injection of the air and the quantity of dissolved oxygen obtained by the aeration process.

In the next step, these results and the detailed bubble flow morphology [12] will be used to validate numerical simulations for dissolved air transfer, to realize the sparger optimization by numerical calculations.

Acknowledgements

This works was performed in the frame of the project NUCLEU PN18240202, ctr. 24N/2018 ElectroEchipaMat, financed by the Ministry of Research and Innovation.

Appendices and nomenclature

A_b [mm^2]	area of an air bubble considered spherical
a [mm^2]	interfacial area of the first swarm of bubbles

a_i [mm^2]	interfacial area of the all bubbles in the system
C [mg/l]	concentration of dissolved oxygen at the moment t
C_0 [mg/l]	concentration of dissolved oxygen at the moment $t = 0$
C_{st} [mg/l]	concentration of dissolved oxygen at saturation, at the surface, at working temperature, at standard pressure of 1 atm, and relative humidity conditions of 100%
C_s [mg/l]	concentration of dissolved oxygen at saturation (estimated by non-linear regression) at working temperatures
C_{s20} [mg/l]	concentration of dissolved oxygen at saturation, corrected at temperature 20°C, at standard pressure of 1 atm, and relative humidity conditions of 100% ($C_{20} = 8.62$ mg/l)
CP	ceramic plate with volume porosity in the range 45–50%
D [mm]	diameter of the plate MP ($D = 44.8$ mm)
DO	dissolved oxygen
d [mm]	diameter of a hole in the plate MP
dp [mwc]	pressure drop on the aerator
GP	fritted (sintered) glass plate with porosity controlled in the range 0.25–0.315 μm
H [m]	hydrostatic head on aerator ($H = 0.8$ m)
g [m/s^2]	gravity
Kla [1/min]	volumetric mass transfer coefficient (estimated by regression)
Kla_{20} [1/min]	Kla, corrected at temperature 20°C
Klat [1/min]	Kla, volumetric mass transfer coefficient at the moment t
Q [m^3/s]	air flow rate injected through the MP
Q_s [m^3/s]	air flow rate at standard conditions: $Q_s = \frac{Q \cdot 273.15}{(273.15 + t_0)}$
MP 0.1–2.4	interchangeable perforated metallic plates with circular holes of 0.1–2.4 mm
N	number of holes on an MP
n_b	number of bubbles in the system $n_b = \frac{V_{voit}}{V_b}$
P [W]	the power consumed for the injection of air through the aerator
P_b [Pa]	atmospheric pressure at the time of testing
Ps [Pa]	standard atmospheric pressure (1 atm)
R_0 [m]	the initial air bubble radius
r_0 [m]	radius of the hole

t [s]	time
t_0 [°C]	air temperature at sampling time
t_w [°C]	water temperature at sampling time
T [s]	air-water contact time
s [mm^2]	active area of intake of the air into the water (sum of the areas of all holes from a an MP)
s′ [%]	active area of intake of the air into the water from an MP
SAE [kgO_2/kWh]	standard aeration efficiency
$SOTE$ [−]	standard oxygen transfer efficiency
$SOTR$ [mg/min]	standard oxygen transfer rate
U [m/s]	theoretical ascending velocity of the bubbles
V [l]	water volume in the tank (V = 72 l)
V_b [l]	volume of an air bubble considered spherical
V_{void} [l]	void volume from the system
W_{O2} [kg/s]	mass flow rate of oxygen from the air stream ($W_{O2} = 0.2765\ Q_s$)
Δp_{tot} [Pa]	total pressure drop (including hydrostatic head), $\Delta p_{tot} = (\Delta p + H)\varrho g$
ε [%]	void fraction
$\tau = C_{st}/C_{20}$ [−]	temperature correction factor
σ [N/m^2]	air-water surface tension coefficient
ϱ [kg/m^3]	water density
θ [−]	empirical temperature correction factor (θ = 1.024, unless another value is proven experimentally)
Ω [−]	pressure correction factor, $\Omega = \frac{P_b}{P_s}$

Author details

Florentina Bunea[1]* and Gabriel Dan Ciocan[2]

*Address all correspondence to: florentina.bunea@icpe-ca.ro

1 National Institute for R&D in Electrical Engineering, ICPE-CA, Romania

2 Laboratoire de Machines Hydrauliques, Laval University, Québec, Canada

References

[1] Bunea F, Bucur DM, Dumitran GE, Ciocan GD. Water quality in hydroelectric sites. In: Voudouris K, ed. Ecological Water Quality-Water Treatment and Reuse. InTech; 2012. pp. 391-408. DOI 10.5772/32078

[2] Bunea F, Ciocan GD, Nedelcu A, Bucur DM, Dunca G, Chihaia R. Experimental setup for the study of new aeration devices in hydraulic turbines. Environmental Engineering and Management Journal. 2017;**16**(5):1033-1040

[3] Fayolle Y, Gillot S, Cockx A, Bensimhon L, Michel R, Alain H: In situ characterization of local hydrodynamic parameters in closed-loop aeration tanks. Chemical Engineering Journal. 2010;**158**:207-212. DOI: 10.1016/j.cej.2009.12.043

[4] Gillot S, Capela S, Héduit A. Alpha Factor and In-Process Efficiency in Horizontal-Flow Aeration Basins, Aeration Conference: Aeration in Deep Basins and Sequencing Batch Reactors. Rome: ITA; 4 May 1998. 11 p

[5] Giovannettone JP, Gulliver JS. Gas transfer and liquid dispersion inside a deep airlift reactor. AIChE Journal. 2008;**54**(4):850-861. DOI: 10.1002/aic.11449

[6] Behin J, Dolati F, Vasseghian Y. Estimation of mass transfer coefficient in different regions of forced circulation airlift loop reactor. In: 7th International Congress on Chemical Engineering; 21-24 November 2011; Kish, Iran

[7] Bunea F, Oprina G, Baran G. Experimental setup for the study of the bubble diffusers hydrodynamic performance. Patent RO 125997 B1, 28.02.2012

[8] Băran G, Băran N. Hidrodinamica bulelor generate de difuzori porosi (hydrodynamics of bubbles generated by porous diffusers). Revista de Chimie. 2003;**54**(5):436-440

[9] ASCE (Standard Measurement of Oxygen Transfer in Clean Water). Measurement of Oxygen Transfer in Clean Water. 2nd ed. American Society of Civil Engineers. Standard no. ANSI/ASCE 2-91/1993. ISBN 087262885x. 45 p

[10] Krishna R, van Baten JM. Mass transfer in bubble columns. Catalysis Today. 2003;**79-80**: 67-75. DOI: 10.1016/S0920-5861(03)00046-4

[11] Krishna R, Van Baten JM, Urseanu MI. Three-phase Eulerian simulations of bubble column reactors operating in the churn-turbulent regime: A scale up strategy. Chemical Engineering Science. 2000;**55**(16):3275-3286. DOI: 10.1016/S0009-2509(99)00582-5

[12] Murgan I, Bunea F, Ciocan GD. Experimental PIV and LIF characterization of a bubble column flow. Flow Measurement and Instrumentation. 2017;**54**:224-235. DOI: 10.1016/j.flowmeasinst.2017.02.004

IntechOpen